Original article

Epileptic Disord 2019; 21 (1): 65-77

A comprehensive clinico-pathological and genetic evaluation of bottom-of-sulcus focal cortical dysplasia in patients with difficult-to-localize focal epilepsy

Zhong Ying [1], Irene Wang [1], Ingmar Blümcke [1,2], Juan Bulacio [1], Andreas Alexopoulos [1], Lara Jehi [1], William Bingaman [1], Jorge Gonzalez-Martinez [1], Katja Kobow [2], Lisa Marie Niestroj [3], Dennis Lal [1,3,4], Konrad Koelble [2], Imad Najm [1]

[1] Epilepsy Center, Cleveland Clinic, Cleveland, Ohio, USA
[2] Neuropathological Institute, University Hospitals Erlangen, Erlangen
[3] Cologne Center for Genomics, University of Cologne, Cologne, Germany
[4] Stanley Center for Psychiatric Research, Broad Institute of Harvard & MIT, Cambridge, Massachusetts, USA

Received October 30, 2017; Accepted November 18, 2018

ABSTRACT – *Aims*. We comprehensively studied the clinical presentation, stereo-EEG and MRI findings, histopathological diagnosis, and brain somatic mutations in a retrospective series of drug-resistant patients with difficult-to-localize epilepsy due to focal cortical dysplasia at the bottom of a sulcus (BOS-FCD).

Methods. We identified 10 patients with BOS-FCD from the Cleveland Clinic epilepsy surgery database submitted for intracranial video-EEG monitoring. Brain MRI, including voxel-based morphometric analysis and surgical tissue submitted for histopathology, was reviewed. Paraffin tissue samples from five patients were made available for targeted next-generation sequencing. Postsurgical follow-up was available in nine patients.

Results. BOS-FCD was identified in the superior frontal sulcus in six patients, inferior frontal sulcus in one patient, central sulcus in one patient, and intraparietal sulcus in two patients. All patients had stereotyped seizures. Intracranial EEG recordings identified ictal onset at the BOS-FCD in all 10 patients, whereas ictal scalp EEG had a localizing value in only six patients. Complete resection was achieved by lesionectomy or focal corticectomy in nine patients. Histopathologically, six patients had FCD type IIb and three had FCD type IIa. Next-generation sequencing analysis of DNA

Correspondence:
Zhong Ying
S51 Epilepsy Center,
Cleveland Clinic,
9500 Euclid Ave,
Cleveland, OH 44195, USA
<yingz@ccf.org>

doi:10.1684/epd.2019.1028

extracted from lesion-enriched (micro-dissected) tissue from five patients with FCD type II led to the identification of a germline frameshift insertion in *DEPDC5,* introducing a premature stop in one patient. Eight out of nine patients with available follow-up were completely seizure-free (Engel Class IA) after a mean follow-up period of six years.
Conclusion. Our results confirm previous studies classifying difficult-to-localize BOS-FCD into the emerging spectrum of FCD ILAE type II mTORopathies. Further studies with large patient numbers and ultra-deep genetic testing may help to bridge the current knowledge gap in genetic aetiologies of FCD.

Key words: brain, seizure, mTOR, epilepsy surgery, outcome

Focal cortical dysplasia (FCD) are common histopathological lesions in children and adults with drug-resistant focal epilepsy (Blümcke *et al*., 2017), and hitherto classified into separate clinico-pathological subtypes (Blümcke *et al*., 2011). However, the aetiology and pathogenesis of most of these subtypes remain to be clarified (Najm *et al*., 2018). Such knowledge will be mandatory to also understand their variable occurrence in size, cellular phenotypes, brain localization and clinical presentation (Krsek *et al*., 2008; Lerner *et al*., 2009; Blümcke *et al*., 2010; Chassoux *et al*., 2012; Harvey *et al*., 2015). Continuous improvement in magnetic field strength for MRI diagnosis and the application of advanced post-processing analyses has significantly enhanced clinical identification of FCD subtypes *in vivo*, in particular, of FCD ILAE type II (Urbach *et al*., 2002; Besson *et al*., 2008; Bernasconi *et al*., 2011; Wagner *et al*., 2011; Mellerio *et al*., 2014; Wang *et al*., 2014). As a pertinent example, hyperintense MRI signalling from the lateral ventricle towards the crown of the gyrus was described as a "transmantle sign" (Barkovich *et al*., 1997), and mostly confirmed in FCD IIb and in the frontal lobe (Colombo *et al*., 2009; Colombo *et al*., 2012). Not all FCD II present, however, with a transmantle sign suggesting a larger clinico-pathological spectrum disorder or even separate disease entities. Two previous reports focused on FCD II located at the bottom of sulcus and highlighted these challenges in neuroimaging, clinical, and electroclinical presentation (Chassoux *et al*., 2012; Harvey *et al*., 2015). Tailored surgical resection was particular favourable, with 87-94% of reported patients (n=57) being completely seizure-free. Intriguingly, about 25% of patients did not reveal abnormal signals at initial MRI examination, and the combination of PET with MRI increased the detection rate (Chassoux *et al*., 2010).
With few exceptions, current research has failed to establish pathology-specific molecular biomarkers that clearly distinguish FCD subtypes (Guerrini *et al*., 2015). In the absence of adequate animal models, surgical brain tissue samples open the unique opportunity to further study tissue-specific signatures. A milestone in FCD research represented the identification of brain somatic mutations, germline mutations, or second-hit mosaic mutations activating the mTOR pathway in surgical brain specimens with histopathology-proven FCD type II (Jamuar *et al*., 2014; Scheffer *et al*., 2014; Baulac *et al*., 2015; D'Gama *et al*., 2015; Lim *et al*., 2015; Mirzaa *et al*., 2016; Moller *et al*., 2016; D'Gama *et al*., 2017; Ribierre *et al*., 2018). With only a third of published cases showing a genetic lesion (Marsan and Baulac, 2018), however, continuous efforts are required to improve our understanding of clinically-meaningful FCD subtypes and successful treatment strategies in the near future. The integration of clinical phenotypes with histopathology and genetic analysis is a powerful option, as recently proposed and already implemented by the WHO for the diagnosis of malignant gliomas and embryonal brain tumours (Louis *et al*., 2016).

Methods

Selection of patients

To investigate patients with difficult-to-localize epilepsy due to cortical dysplasia at the bottom of sulcus, we retrospectively reviewed the Cleveland Clinic Epilepsy Center's surgery database with patients who underwent invasive intracranial studies from 2004 to 2014 (as approved by the Cleveland Clinic Institutional Review Board). Inclusion of patients was based on the following criteria:
– drug-resistant focal epilepsy;
– a single MRI lesion restricted to the bottom of a sulcus;
– no previous epilepsy surgery;
– intracranial video-EEG monitoring prior to surgery;
– no concomitant other diagnosis, such as tuberous sclerosis or brain tumour;
– post-operative MRI available to assess the extent of the resection;
– and histopathology slides available for post hoc microscopic review.

Magnetic resonance imaging (MRI)

Four patients were imaged with a 3 T Siemens Trio/Skyra scanner (Erlangen, Germany) and six

patients with a 1.5 T Siemens Avanto scanner (Erlangen, Germany). Sequence parameters at 3 T were: repetition time = 1,860 milliseconds, echo time = 3.4 milliseconds, inversion time = 1,100 milliseconds, flip angle = 10 degrees, band width = 130 kHz, slice thickness = 0.94 mm, no gap, and a 256 × 256 matrix providing isotropic voxels of 0.94 mm. Sequence parameters at 1.5 T were: repetition time = 11 milliseconds, echo time = 4.6 milliseconds, no inversion, flip angle = 20 degrees, band width = 130 kHz, slice thickness = 1.25 mm, no gap, and a 256 × 256 matrix providing 0.9 mm in-plane resolution. All MR images were reviewed by experienced board-certified neuroradiologists specialized in epileptology. Morphometric MRI analysis was available in one patient at the time of surgical evaluation and was retrospectively processed in the remaining nine patients. A voxel-based morphometric analysis program (MAP) was carried out in SPM (Wellcome Department of Cognitive Neurology, London, UK) and Matlab (MathWorks, Natick, Massachusetts) following established protocols (Huppertz *et al*., 2005). MAP was performed on T1-weighted MPRAGE sequence, and the grey-white junction output was examined in each patient with a z-score threshold of 4; the choice of threshold was consistent with previous reports (Wang *et al*., 2014, 2015) (*figure 1*). All 10 patients had FDG-PET. Ictal SPECT was successfully accomplished in six patients and subtraction ictal SPECT coregistered with MRI (SISCOM) was performed.

Neurophysiology

All patients had continuous scalp video-EEG monitoring to confirm the focal epilepsy and characterize the seizure semiology (*table 1*). Following the initial non-invasive evaluation, a recommendation for an invasive intracranial video-EEG evaluation was made during the Cleveland Clinic Epilepsy Center multidisciplinary patient management conference in all 10 patients for three reasons:

– ictal EEG findings and FDG-PET or ictal SPECT was discordant in five patients (*table 1*);

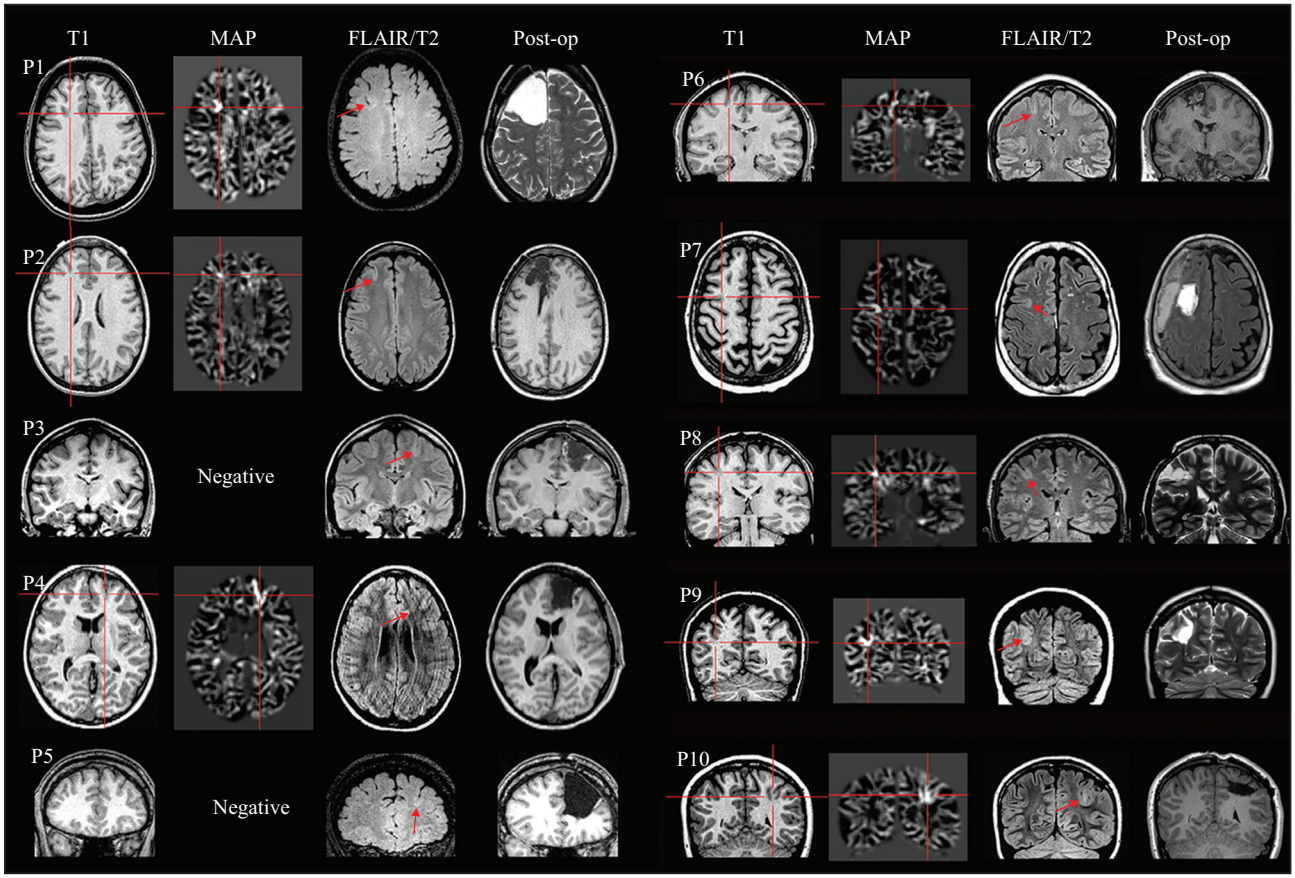

Figure 1. MRI findings and post-processing results for all patients included in the study. The first two columns are the preoperative T1w MPRAGE images and the coregistered MAP grey-white junction output. The crosshair pinpoints the location of the lesion. Absence of the MAP junction image indicates that the MAP processing was negative. The third column is the preoperative FLAIR/T2 images, whichever best depict the lesion (shown by arrow) in that particular patient. The rightmost column shows the postoperative MRI, indicating the extent of resection of the lesions.

Table 1. Detailed demographics and clinical data.

Pt	Age onset (yr)	Age surgery (yr)	MRI	MAP	Other presurgical studies	Seizure semiology	Scalp EEG SZ, interictal SW	Why intra-cranial VEEG?	Intracranial video-EEG	Surgery	Pathology/ Genetics	Outcome	Follow-up (yrs)
1	0.75	46	Right SFS	+	PET: non-contributory Ictal SPECT: concordant	Complex motor ->2nd GTC	SZ: non-localizable SW: none	Scalp EEG seizure non-localizable	SDG+depth	Focal CTX	FCD IIa	Engel IA	5
2	12	35	Right SFS	+	Ictal SPECT and PET: concordant	Non-specific aura -> axial tonic ->complex motor	SZ: non-localizable SW: none	Scalp EEG seizure non-localizable	SDG+depth	LTX	FCD IIb FFPE (10.07%)	Engel IA	5
3	4	20	Left SFS	-	PET: concordant. Ictal SPECT: non-contributory	Non-specific aura -> asymmetric tonic -> right arm clonic	SZ: vertex region SW: vertex, and left centro-parietal	Scalp EEG seizure non-lateralizing	SDG	LTX	FCD IIb FFPE (10.47%)	Engel IA	11
4	1.5	13	Left SFS	+	PET: discordant Ictal SPECT: unsuccess-ful	Right versive -> asymmetric tonic -> 2nd GTC	SZ: left frontal SW: left frontal, left frontal polar	Discordant PET findings	SDG+depth	Focal CTX	FCD IIa FFPE (7.01%) *DEPDC5*	Engel IA	9
5	9	37	Left SFS	-	Ictal SEPCT and PET: concordant with subtle abnormal findings on MRI	Complex motor	SZ (1) left frontal and central; (2) non-localizable SW: none	MRI lesion not clear	SDG+depth	Focal CTX	FCD IIb FFPE (7.79%)	Engel IA	6.5
6	8	29	Right SFS	+	Ictal SPECT and PET : discordant MEG: normal	Head turning to right then left arm elevation	SZ: vertex region and maximum right central; SW: none	Discordant semiology and MRI lesion	SDG+depth	LTX	FCD IIa	Engel IA	2.5

Table 1. Detailed demographics and clinical data (*Continued*).

Pt	Age onset (yr)	Age surgery (yr)	MRI	MAP	Other presurgical studies	Seizure semiology	Scalp EEG SZ, interictal SW	Why intra-cranial VEEG?	Intracranial video-EEG	Surgery	Pathology/ Genetics	Outcome	Follow-up (yrs)
7	13	59	Right IFS	+	PET: non-contributory Ictal SPECT: concordant	Non-specific aura -> left eye/head tonic -> left versive -> 2nd GTC	SZ: (1) right temporo-parietal; (2) right frontocentral; SW: right frontocentral	Functional mapping	SDG+depth	LTX	FCD IIb	NA	NA
8	5	33	Right CS	+	PET: non-contributory Ictal SPECT: unsuccessful	Non-specific aura in left eye -> left face/arm tonic -> 2nd GTC	SZ: right central SW: none	Functional mapping	SEEG	LTX	Small fragment	Engel IA	5.25
9	14	23	Right IPS	+	PET: concordant	Complex visual aura -> dialeptic	SZ: right parieto occipital; SW: right parieto-occipital, posterior temporal	Determine margins of resection	SDG+depth	LTX	FCD IIb FFPE (7.78%)	Engel IA	4.25
10	12	13	Left IPs	+	PET: concordant	Non-specific aura with visual component -> right arm tonic, tonic-clonic -> 2nd GTC	SZ: left centro-parietal SW: left centro-parietal	Functional mapping	SDG+depth	Incomplete LTX	FCD IIb	Engel III	2 months

Pt: patient; yr: year; SFS: superior frontal sulcus; IFS: inferior frontal sulcus; CS: central sulcus; IPS: intra-parietal sulcus; MAP: morphometric analysis program (retrospectively processed in nine patients [Patients 1-9] and not available at the time of surgical evaluation); SDG+depth: subdural grids plus depth electrodes; CTX: corticoectomy; LTX: lesionectomy; SZ: ictal EEG seizure; SW: interictal sharp wave; FFPE: formalin-fixed, paraffin-embedded. Genetic studies were performed in Patients 2, 3, 4, 5 and 9 (numbers within parentheses indicate percentages of dysplastic cells).

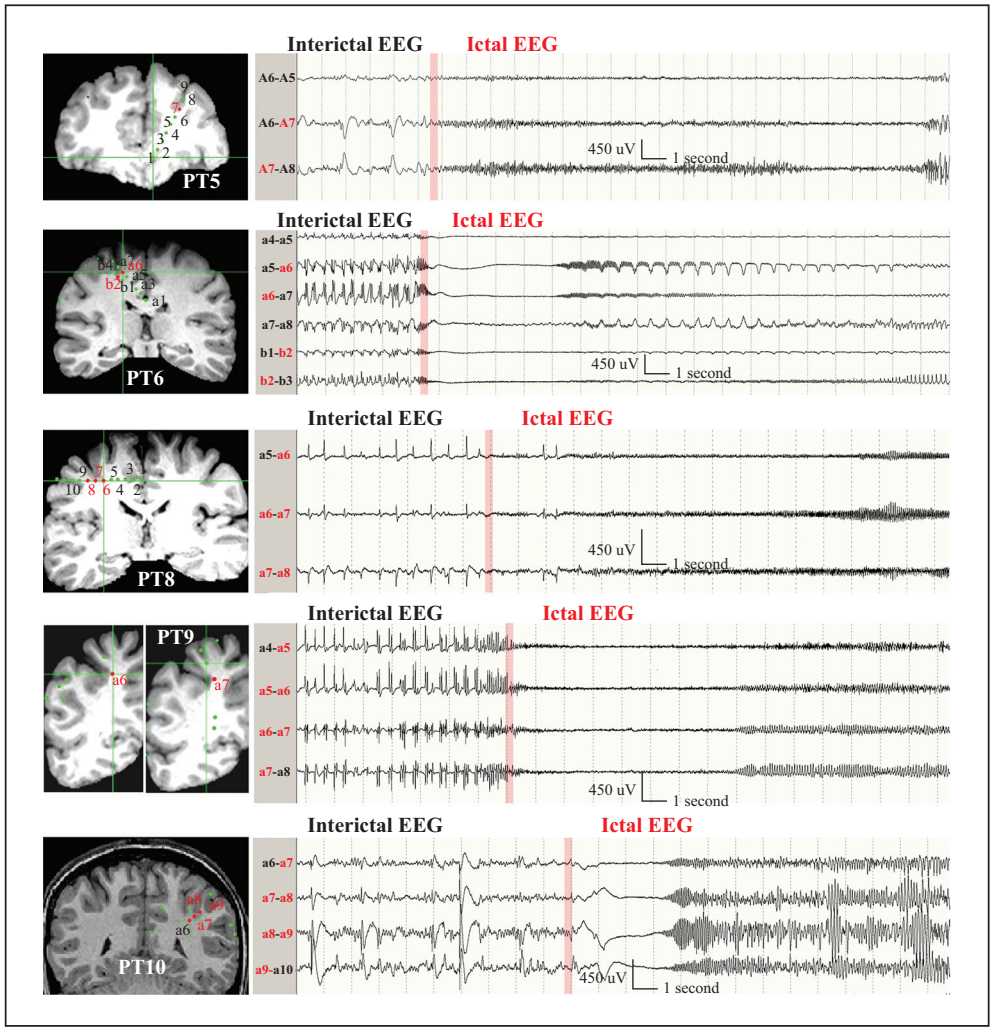

Figure 2. Location of the depth electrode contacts and their anatomic relation to BOS lesions as co-registered on T1-weighted MRI coronal cuts in five patients are shown on the left. The electrode contacts recording ictal EEG onset are labelled in red. The samples of EEG channels recording ictal EEG onset from the depth electrodes (bipolar montage) are shown on the right. The red bars point to the ictal EEG onsets that were preceded by the preictal repetitive spikes/polyspikes in each of the patients. Patients (PT) 6 and 9 showed interictal rhythmic polyspikes and wave discharges that became more frequent immediately prior to the ictal onset. Patients 5 and 10 showed interictal repetitive spikes that were intermixed with low-voltage fast activities. In all patients, ictal EEGs showed tonic fast-frequency discharges. Seizures in Patients 6 and 10 were characterized by a brief initial attenuation of the EEG prior to the emergence of the low-amplitude fast activities.

– eloquent cortical areas had to be mapped for the definition of surgical resection borders in four patients;
– and BOS-FCD was not unambiguously accepted by the group in one patient (Patient 5) (*table 1*).

Eight patients had an implantation of subdural grid electrodes (SDG) together with intracerebral depth electrodes targeting the BOS-FCD of interest. The placement of depth electrodes and their 3D spatial correlation with the MRI-identified lesion was verified through co-registration of post-implantation volume acquisition CT scans and preimplantation high-resolution MRI volume acquisition sequences (*figure 2*). One patient had SDGs without depth electrode implantation (Patient 3) (*table 1*). Patient 8 had stereotactic implantation of depth electrodes according to the SEEG methodology, as previously described (Gonzalez-Martinez *et al.*, 2014).

Neurosurgery

Surgical resection strategies were discussed following the invasive evaluation at our patient management conference, integrating all available data from MRI analysis and neurophysiological recordings. *Post hoc* analysis of the extent of surgical resection was obtained from post-surgical MRI. Post-operative

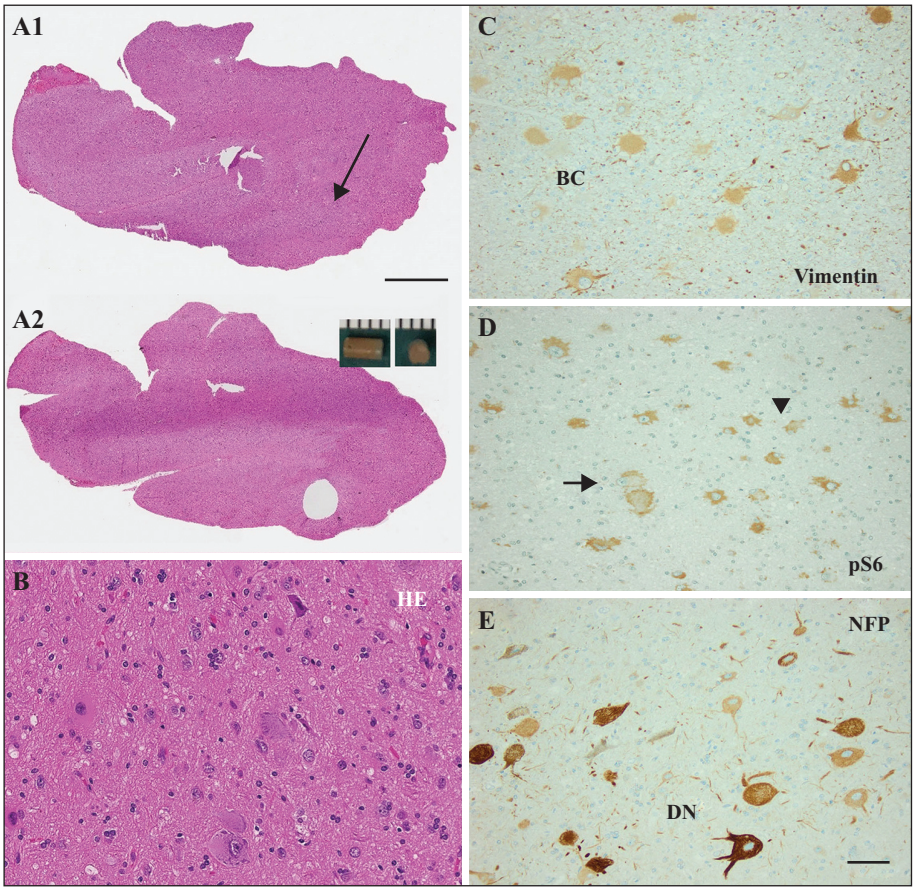

Figure 3. (A-C) H&E staining: whole-slide imaging of Patient 9 (*table 1*) before (A1) and after (A2) microdissection with a 2-mm diameter punching device (scale bar = 4 mm); (B) higher magnification of area indicated by arrow in (A) and used for DNA extraction following micro-dissection (shown in [A']). (C) Vimentin immunohistochemistry highlighting balloon cells (BC); serial section from (B). (D) phosphorylated S6 (pS6) immunohistochemistry highlighting both FCD II cell types, dysmorphic neurons (arrow), and balloon cells (arrowheads); serial section from (B). (E) Immunohistochemistry for neurofilament protein highlighting dysmorphic neurons (DN); serial section from (B). Microscopic measurements reveal 8% of cells with a FCDII phenotype. Scale bar in (B-E) = 50 μm.

seizure outcome was assessed during regular outpatient visits using Engel's classification scale (Engel *et al*., 1993).

Immunohistochemistry

For histopathological diagnosis, surgical specimens were formalin-fixed and paraffin-embedded. Post hoc review of all surgical tissue was based on immunohistochemical stainings to visualize architectural dysplasia (Blümcke *et al*., 2016) using antibodies directed against NeuN (clone A60, Chemicon, USA) and MAP2 (clone HM2, DAKO, Denmark), to visualize dysmorphic neurons with antibodies directed against non-phosphorylated neurofilaments (clone SMI32, Covance, USA) or balloon cells with antibodies directed against vimentin (polyclonal antibody V9, DAKO, Denmark) (*see also* Blümcke *et al*. [2016]). Immunohistochemical detection of the phospho-S6 epitope (clone ser235/236, Cell Signaling Technology, USA) was used to demonstrate an activated mTOR pathway. Areas with highest content of abnormal cells were identified on the H&E section, and the same area labelled in the FFPE bloc. In nine patients, FFPE tissue was micro-dissected using a 2-mm diameter large punching needle (*figure 3*). DNA extraction from the FFPE tissue punch was performed using customized protocols for small FFPE tissue (Qiagen, Germany) with sufficient DNA available for deep sequencing in five patients. Semi-quantitative cell measurements were performed as following: a HE stained section was prepared before and after the tissue punch and fully digitized using whole slide digital imaging (3DHistech, Hungary). All cells within 1 mm^2 of the punched area were counted from the computer screen (range: 171-673 cells). FCD-specific cells referred to dysmorphic neurons in FCD IIa and IIb and balloon cells in FCD IIb and were counted from the same region of interest (range: 18-80 cells). Results were expressed as percentage of FCD-specific from total cells.

Genetic analysis

To perform the targeted sequencing, we used the Agilent SureSelect Custom Enrichment Kit for library preparation of 166 self-selected genes. Library preparation was conducted according to the manufacturer's protocols and subsequent paired-end library sequencing was performed using the Illumina HiSeq4000. The targeted genes included those encoding proteins of the mTOR and PI3K-AKT signalling pathway, genes associated with low-grade brain tumours, and genes associated with epilepsy. The list of mTOR pathway genes was derived from the Kegg Pathway (ID: hsa04150). The PI3K-AKT pathway genes were derived from RT2 Profiler PCR Array (Qiagen, Product no.: 330231). Genes associated with low-grade brain tumours were derived from the recent literature and epilepsy genes were derived from the EpiPM Consortium review in 2015 (Vogelstein *et al.*, 2013; EpiPMConsortium, 2015). The full list of included genes is disclosed in *supplementary table 1*.

For bioinformatic analysis, we generated analysis-ready bam files using BWA to map reads to the human genome reference build GRCh37 (Li and Durbin, 2009). GATK was used to mark duplicated reads (McKenna *et al.*, 2010), perform local realignment, recalibrate the base quality scores, and call SNPs and short indels together with SAM tools and Dindel (Li *et al.*, 2009; Albers *et al.*, 2011). In addition, we used Platypus to call low allele frequency variants (Rimmer *et al.*, 2014). We used the human reference genome build GRCh37 and annotated variant functional consequences and population allele frequencies using wANNOVAR (excessed: 12/2016; http://wannovar.wglab.org). We removed non-protein-coding variants and variants present in individuals from the general population with allele frequency >0.1% to enrich for rare variants of large effect. Variants passing our applied filters, were manually inspected for sequencing and variant calling quality using the Integrative Genomics Viewer (Robinson *et al.*, 2011). The manual evaluation was conducted by three independent scientists. Variant pathogenicity was assessed in accordance with 28 criteria defined by guidelines of the American College of Medical Genetics and Genomics (ACMG) (Richards *et al.*, 2015). We used the online tool, InterVar, to facilitate the variant interpretation process (Li and Wang, 2017).

Results

Patient data

Ten patients fulfilled our inclusion criteria; four males and six females. None of the patients had any neurological deficit at clinical examination. One patient had mild developmental delay (Patient 4) (*table 1*). All patients presented with stereotyped seizures (*see table 1*), without a history of *status epilepticus*, infantile spasms or febrile seizures. Age at epilepsy onset ranged from 0.75 to 14 years (mean: 7.2 years). Age at time of surgery ranged from 13 to 59 years (mean: 33.2 years). Epilepsy duration was between one and 46 years (mean: 23.4 years). None of the patients had a history of pre- or perinatal injuries except for one patient who was born two months premature (Patient 7) (*table 1*). Clinical histories and seizure description of all patients included in the study are summarized in *table 1*.

Imaging data

BOS-FCD was identified in all patients by epilepsy expert neuroradiology review (*figure 1*). Six lesions were located in the superior frontal sulcus, one lesion in the inferior frontal sulcus, one lesion in the central sulcus, and two lesions in the intraparietal sulcus. Focal cortical thickening and blurring of the grey-white matter junction at the bottom of a sulcus was a common MRI finding in all patients, as illustrated in *figure 1*. These abnormalities were best visible on FLAIR sequences. Eight out of 10 patients had concordant signal changes on T1w images (*figure 1*). Blurring of the grey-white matter junction was evident on T1w images in four patients by visual inspection (Patients 1, 4, 9, and 10) (*table 1*), and eight patients showed positive MAP foci. Blurring of the grey-white matter junction on T1w images became evident in four patients only after MAP analysis with a z-score set >4 (Patients 2, 6, 7, and 8). No T1w signal changes were observed visually or by MAP analysis in the remaining two patients (Patients 3 and 5). A funnel-shaped, subcortical hyper-intensity tapering abnormality towards the ventricular surface (transmantle sign) was seen in three patients (Patients 1, 8 and 9) (*see figure 1*).

Scalp video-EEG monitoring

Habitual seizures were documented in all patients by scalp video-EEG-monitoring. Semiology could not be, however, correlated simply with lobar location of the BOS-FCD (*table 1*). As an example, most of the auras were non-specific. Secondly, presence of auras with eye involvement could be anatomically misleading in both patients (Patients 9 and 10) with intraparietal BOS-FCD. Ictal EEG patterns were non-localizable in two patients (Patients 1 and 2) (*table 1*), regional lobar for two patients in one brain region (Patients 4 and 8) and for two patients with two adjacent brain regions

(Patients 9 and 10), and at the midline vertex region in two patients (Patients 3 and 6). Interictal sharp waves were absent in five patients and did not add localizing value in non-localizing ictal EEGs.

FDG-PET and ictal SPECT

Interictal FDG-PET studies were performed in all patients (*table 1*); only five out of 10 patients exhibited focal hypometabolism concordant with the lesion detected by MRI, whereas the remaining five patients had non-contributory results, including two patients with discordant PET localization. In four out of six patients with successful ictal SPECT and SISCOM, the area of hyperperfusion was concordant with the MRI-visible BOS-FCD (*table 1*).

Invasive video-EEG monitoring

At the time of surgical evaluation, all 10 patients proceeded to invasive EEG evaluation based on the decision of the patient management conference at that time (*table 1*): non-localizing ictal EEG in three patients, atypical semiology associated with the lesion in one patient, MRI lesion was not unanimously convinced by the committee in one patient, discordant PET hypometabolism in one patient, and functional mapping was recommended in four patients.

Habitual seizures were documented in all patients also by invasive video-EEG monitoring. Ictal EEG onset was mapped to depth electrode contacts localized in the BOS-FCD or in areas sampled adjacent to the lesion in eight patients (*figure 2*). In the remaining two patients (Patient 2 with no depth electrode contacts in the proximity of the lesion or depth of sulcus, and Patient 3 with SDG electrodes only), ictal EEG onset was recorded from electrodes placed in the gyral crown of the sulci harbouring the lesion.

The depth electrodes were located within or in close vicinity to the BOS-FCD in seven patients (*table 1*). Only in Patient 2, co-registration revealed the depth electrode not inside or close to the lesion. Histopathology analysis confirmed the iEEG trajectory in close vicinity to the FCD in one patient (data not shown). Intracranial EEG recordings with depth electrode contacts in bottom-of-sulcus lesions showed continuous interictal discharge patterns consisting of rhythmic (1-3-Hz) spikes/polyspikes and waves. The rhythmic spiking pattern was intermixed with low-amplitude fast discharges (*figure 2*). Extraoperative video and EEG recordings captured the patients' typical clinical seizures with stereotyped ictal EEG onset patterns that were localized at the depth electrode contacts in or near the BOS-FCD (*figure 2, also in reference to figure 1*). All EEG seizures transitioned from continuous pre-ictal rhythmic epileptiform discharges to tonic fast frequency discharges of variable voltage for durations ranging from 15 to 25 seconds (*figure 2*).

Surgical resection and seizure outcome

Neurosurgical resection of the lesion was limited to overlying and surrounding cortex (*i.e.* lesionectomy) in seven patients and corticoectomy with resection of the lesion plus adjacent gyri was performed in three patients (*table 1*). *Figure 1* illustrates the anatomy of the resection in all patients (post-operative MRI). Eight patients became free of seizures and auras (Engel Class 1A) (*table 1*) with a mean follow-up time of six years (2.5 years to 11 years). One patient (Patient 7) did not return for follow-up. One patient (Patient 10) had incomplete resection due to the epileptic zone overlapping with eloquent cortex, as determined by extraoperative brain stimulation via subdural grids and depth electrodes, and this patient continued to have seizures (Engel Class III).

Histopathological findings

All surgical specimens were histopathologically and immunohistochemically reviewed and classified as FCD ILAE type II, with a combination of dysmorphic neurons and balloon cells (FCD IIb) in six patients and dysmorphic neurons only (FCD IIa) in three patients (*table 1*). Only small tissue fragments were submitted for pathological examination in one patient and microscopic review remained inconclusive (Patient 8). The gross neuroanatomical presentation of FCD IIb can be demonstrated best using immunohistochemical labelling of surgically well-preserved specimens with the characteristic presentation of vimentin-immunoreactive balloon cells and neurofilament-accumulating dysmorphic neurons (*figures 3, 4*). In addition, immunohistochemical labelling of the phospho-S6 epitope revealed specific staining in all specimens.

Genetic findings

Targeted next-generation sequencing (NGS) achieved a mean coverage of 245 × (SD = 60) across the target genes, with 96.3% (SD = 0.95) of bases covered at 50 × (*supplementary table 1*). The microdissected patient samples harboured a mean fraction of dysplastic cells of 8.6% (SD=1.4). Given our sequencing coverage and the assumption that all dysplastic cells should carry the variant, we would have been able to detect 99% of all brain somatic variants with Platypus in these cells (Richards *et al.*, 2015). We screened for coding variants in 166

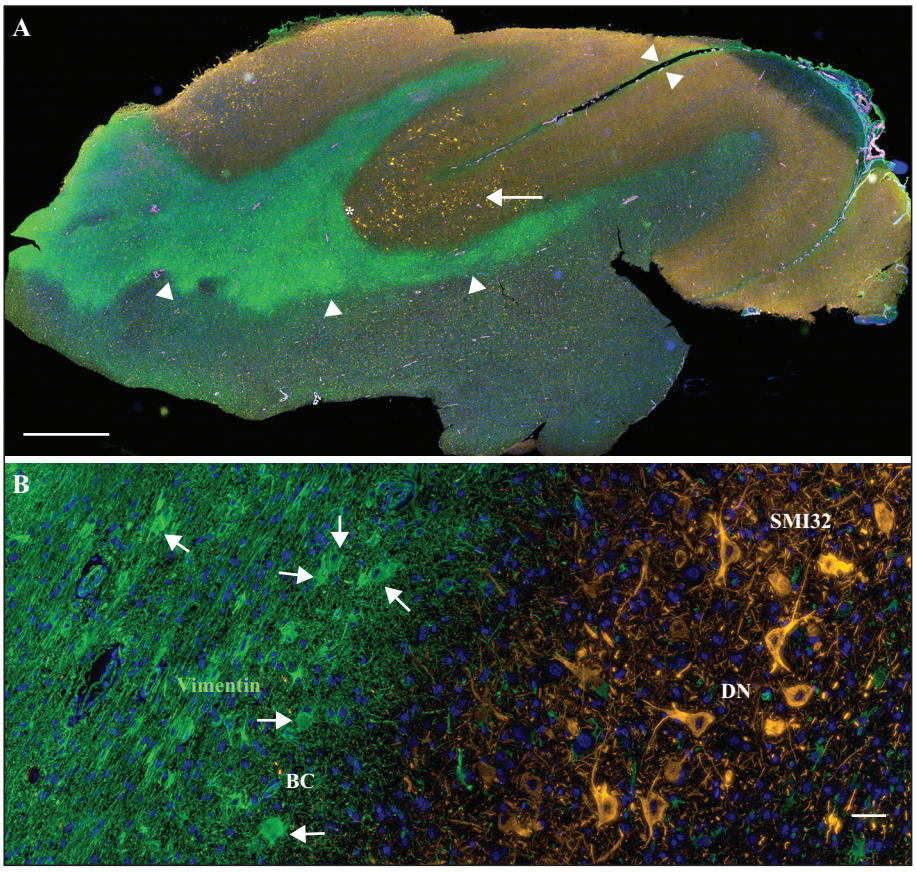

Figure 4. Surgical histopathology of Patient 9 (*table 1*). (A) Concentration of dysmorphic neurons (arrow) decorated with anti-non-phosphorylated neurofilament H-specific antibodies (clone SMI32, Alexa555-labeled anti-mouse IgG1 secondary antibody, orange pseudocolour) at the bottom of a sulcus (sulcal surface indicated by small arrowheads), with concomitant accumulation of vimentin-positive balloon cells (clone SP20, Alexa488-labeled anti-rabbit IgG secondary antibody, green pseudocolour; arrowheads) in the underlying white matter. In addition, vascular myocytes expressing smooth muscle actin (clone 1A4, Alexa647-labelled anti-murine IgG2a secondary antibody, magenta pseudocolour) and nuclei (Hoechst 33342, blue pseudocolour) are visualized (multichannel-immunofluorescence whole slide imaging, 3DHistech MIDI). (B) High-power magnification of area indicated by asterisk in (A) showing predominant localization of vimentin-immunopositive balloon cells (BC) in white matter (as indicated by arrows) and SMI32-immunopositive dysmorphic neurons (DN) in grey matter. Scale bar in (A) = 2 mm, in (B) = 50 μm.

candidate genes (*supplementary table 1*) and did not identify brain somatic variants. DNA obtained from blood leucocytes was, however, not available in this retrospective analysis to confirm germline origin. The variants were identified in eight genes and comprised nine exonic heterozygous missense variants (mean allele frequency = 47%; SD = 3.6) and one frameshift insertion introducing a stop codon. All nine missense variants were classified as 'variants of uncertain significance' (VUS) using state-of-the-art guidelines in the field (Richards *et al.*, 2015). The frameshift insertion (NM_001136029, p.Asp1075Glufs*3) introduces a premature stop codon in *DEPDC5*, likely leading to haploinsufficiency and was classified as 'likely pathogenic' for the epilepsy according to recommended ACMG guidelines and current epilepsy literature (Ishida *et al.*, 2013; Lal *et al.*, 2014; Epi4Kconsortium, 2017).

Discussion

Our comprehensive analysis of 10 patients with difficult-to-localize BOS-FCD confirms previous studies with a "syndromic description" of FCD ILAE type II:

– seizure onset at preschool or school age;
– mostly of frontal localization;
– stereotyped seizures;
– distinct MRI features;
– intrinsic epileptogenicity;
– favourable postsurgical seizure outcome following complete resection of the epileptic region;
– and exclusivity of FCD type II with immunohistochemical or genetic evidence for activation of the mTOR pathway.

The fact that FCD-BOS lesions are small and localized to the bottom of sulcus suggested, however, a later

occurrence of a (presumably) genetically acquired pathogen during the estimated 32 mitotic cycles of cortical brain development, compared to FCD II lesions involving a larger cortical area or extending even to hemimegalencephaly (D'Gama *et al*., 2017; Blümcke and Sarnat, 2016).

NGS analysis of a panel of 166 mTor, PIK3/Akt, and other epilepsy-related genes detected a likely pathogenic, epilepsy-associated variant in *DEPDC5* (terminology used according to ACMG guidelines) in only one out of five patients studied. This is consistent with previous studies, which reported 'likely pathogenic' variants in mTOR pathway-associated genes in only 25% (SD=40) of patients with histopathologically confirmed FCD II (Marsan and Baulac, 2018). The majority of variants have been reported as brain somatic with allele frequencies of 1-12.6%, and predominantly affecting the *MTOR* gene (Baulac *et al*., 2015; D'Gama *et al*., 2015; Lim *et al*., 2015; Mirzaa *et al*., 2016; Moller *et al*., 2016; D'Gama *et al*., 2017). One study reported germline *DEPDC5* mutations in cases of BOS-FCD, which further stressed the association with mTORopathies (Scheffer *et al*., 2014). Recently described second-hit mosaic mutations may be another etiologic pathomechanism to be taken into consideration (Ribierre *et al*., 2018). In our present study, we detected a new pathogenic *DEPDC5* heterozygous variant in one patient with FCD IIa. Stop codon-inducing germline variants in *DEPDC5* have recently been shown to be present in 3% of patients (cohort: n=1187) with familial non-acquired focal epilepsy without cortical structural abnormalities and only in 0.05% of controls (cohort: n=3877; $p=9.6 \times 10^{-12}$) (Epi4Kconsortium, 2017). In addition, one study identified a somatic mutation in *DEPDC5* in addition to an existing germline mutation (Baulac *et al*., 2015). The *DEPDC*5 variant identified in this study had an allele frequency of 41%. However, only 8.6% (SD=1.4) of cells shared a dysplastic phenotype by microscopic review, indicating that the identified p.Asp1075Glufs*3 *DEPDC5* variant is unlikely to be only present in dysplastic cells. Unfortunately, we were not able to validate this prediction because blood samples were not available retrospectively. Further studies should clarify whether this *DEPDC5* variant is causal for the epilepsy or if the epilepsy is secondary to FCDII. In all other BOS-FCD patients, no likely pathogenic or pathogenic variant was identified. However, our NGS coverage was, for the majority of samples, higher compared to previous reports (median: 243.72x *vs*. 180x), which should enable us to detect 99% of all somatic variants with variant allele frequencies of $> 8\%$. Our results call for extended molecular/genetic investigations integrating ultra-deep exome-wide DNA and single-cell RNA sequencing, as well as methylome and proteomic analysis to identify a possible pathogenic cause(s). Future progress in precision medicine will build on such analysis to develop a targeted drug treatment for specific mTOR signalling molecules, in particular, when epilepsy surgery is not an option for a given patient.

Despite the fact that our study addressed only a small number of patients and any conclusion would need confirmation by larger and prospectively collected patient series, the comprehensive approach integrating genotype with phenotype analysis will help to consolidate the recognition of FCD-BOS in focal and difficult-to-localize epilepsies. Re-review of MRI and application of post-processing methodologies led to the identification of cortical dysplasia at BOS localization in all our patients, most often in the frontal or parietal lobes. Favourable outcome after neurosurgical resection, histopathological diagnosis of FCD II, and genetic testing helped to validate the clinical hypothesis. No other diagnostic modality added significant value in clinical management, as seen from a retrospective angle. In the future, MRI fingerprinting is the resolution for this population of patients (Ma *et al*., 2013). □

Supplementary data.

Supplementary table is available on the www.epilepticdisorders.com website.

Acknowledgements and disclosures.

The work was supported by the European Union (FP7 DESIRE GA # 602531). We are thankful to Emily Kiefer (Cleveland) and Birte Rings (Erlangen) for their expert technical assistance.

None of the authors have any conflict of interest to declare.

References

Albers CA, Lunter G, MacArthur DG, McVean G, Ouwehand WH, Durbin R. Dindel: accurate indel calls from short-read data. *Genome Res* 2011; 21: 961-73.

Barkovich AJ, Kuzniecky RI, Bollen AW, Grant PE. Focal transmantle dysplasia: a specific malformation of cortical development. *Neurology* 1997; 49: 1148-52.

Baulac S, Ishida S, Marsan E, *et al*. Familial focal epilepsy with focal cortical dysplasia due to *DEPDC5* mutations. *Ann Neurol* 2015; 77: 675-83.

Bernasconi A, Bernasconi N, Bernhardt BC, Schrader D. Advances in MRI for 'cryptogenic' epilepsies. *Nat Rev Neurol* 2011; 7: 99-108.

Besson P, Andermann F, Dubeau F, Bernasconi A. Small focal cortical dysplasia lesions are located at the bottom of a deep sulcus. *Brain* 2008; 131: 3246-55.

Blümcke I, Sarnat HB. Somatic mutations rather than viral infection classify focal cortical dysplasia type II as mTORopathy. *Curr Opin Neurol* 2016; 29: 388-95.

Blümcke I, Pieper T, Pauli E, *et al*. A distinct variant of focal cortical dysplasia type I characterised by magnetic resonance imaging and neuropathological examination in children with severe epilepsies. *Epileptic Disord* 2010; 12: 172-80.

Blümcke I, Thom M, Aronica E, *et al*. The clinico-pathological spectrum of focal cortical dysplasias: a consensus classification proposed by an ad hoc Task Force of the ILAE Diagnostic Methods Commission. *Epilepsia* 2011; 52: 158-74.

Blümcke I, Aronica E, Miyata H, *et al*. International recommendation for a comprehensive neuropathologic workup of epilepsy surgery brain tissue: a consensus Task Force report from the ILAE Commission on Diagnostic Methods. *Epilepsia* 2016; 57: 348-58.

Blümcke I, Spreafico R, Haaker G, *et al*. Histopathological findings in brain tissue obtained during epilepsy surgery. *New Engl J Med* 2017; 377: 1648-56.

Chassoux F, Rodrigo S, Semah F, *et al*. FDG-PET improves surgical outcome in negative MRI Taylor-type focal cortical dysplasias. *Neurology* 2010; 75: 2168-75.

Chassoux F, Landre E, Mellerio C, *et al*. Type II focal cortical dysplasia: electroclinical phenotype and surgical outcome related to imaging. *Epilepsia* 2012; 53: 349-58.

Colombo N, Salamon N, Raybaud C, Ozkara C, Barkovich AJ. Imaging of malformations of cortical development. *Epileptic Disord* 2009; 11: 194-205.

Colombo N, Tassi L, Deleo F, *et al*. Focal cortical dysplasia type IIa and IIb: MRI aspects in 118 cases proven by histopathology. *Neuroradiology* 2012; 54: 1065-77.

D'Gama AM, Geng Y, Couto JA, *et al*. Mammalian target of rapamycin pathway mutations cause hemimegalencephaly and focal cortical dysplasia. *Ann Neurol* 2015; 77: 720-5.

D'Gama AM, Woodworth MB, Hossain AA, *et al*. Somatic mutations activating the mtor pathway in dorsal telencephalic progenitors cause a continuum of cortical dysplasias. *Cell Rep* 2017; 21: 3754-66.

Engel J Jr, Van Ness PC, Rasmussen TB, Ojemann LM. Outcome with respect to epileptic seizures. In: *Surgical treatment of the epilepsies*. Engel J Jr. New York: Raven Press, 1993.

EpiPMConsortium. A roadmap for precision medicine in the epilepsies. *Lancet Neurol* 2015; 14: 1219-28.

Epi4Kconsortium. Ultra-rare genetic variation in common epilepsies: a case-control sequencing study. *Lancet Neurol* 2017; 16: 135-43.

Gonzalez-Martinez J, Mullin J, Bulacio J, *et al*. Stereoelectroencephalography in children and adolescents with difficult-to-localize refractory focal epilepsy. *Neurosurgery* 2014; 75: 258-68, discussion: 67-8.

Guerrini R, Duchowny M, Jayakar P, *et al*. Diagnostic methods and treatment options for focal cortical dysplasia. *Epilepsia* 2015; 56: 1669-86.

Harvey AS, Mandelstam SA, Maixner WJ, *et al*. The surgically remediable syndrome of epilepsy associated with bottom-of-sulcus dysplasia. *Neurology* 2015; 84: 2021-8.

Huppertz HJ, Grimm C, Fauser S, *et al*. Enhanced visualization of blurred gray-white matter junctions in focal cortical dysplasia by voxel-based 3D MRI analysis. *Epilepsy Res* 2005; 67: 35-50.

Ishida S, Picard F, Rudolf G, *et al*. Mutations of *DEPDC5* cause autosomal dominant focal epilepsies. *Nat Genet* 2013; 45: 552-5.

Jamuar SS, Lam AT, Kircher M, *et al*. Somatic mutations in cerebral cortical malformations. *New Engl J Med* 2014; 371: 733-43.

Krsek P, Maton B, Korman B, *et al*. Different features of histopathological subtypes of pediatric focal cortical dysplasia. *Ann Neurol* 2008; 63: 758-69.

Lal D, Reinthaler EM, Schubert J, *et al*. *DEPDC5* mutations in genetic focal epilepsies of childhood. *Ann Neurol* 2014; 75: 788-92.

Lerner JT, Salamon N, Hauptman JS, *et al*. Assessment and surgical outcomes for mild type I and severe type II cortical dysplasia: a critical review and the UCLA experience. *Epilepsia* 2009; 50: 1310-35.

Li H, Durbin R. Fast and accurate short read alignment with Burrows-Wheeler transform. *Bioinformatics* 2009; 25: 1754-60.

Li Q, Wang K. InterVar: clinical interpretation of genetic variants by the 2015 ACMG-AMP Guidelines. *Am J Hum Genet* 2017; 100: 267-80.

Li H, Handsaker B, Wysoker A, *et al*. The sequence alignment/map format and SAMtools. *Bioinformatics* 2009; 25: 2078-9.

Lim JS, Kim WI, Kang HC, *et al*. Brain somatic mutations in MTOR cause focal cortical dysplasia type II leading to intractable epilepsy. *Nature Med* 2015; 21: 395-400.

Louis DN, Perry A, Reifenberger G, *et al*. The 2016 World Health Organization classification of tumors of the central nervous system: a summary. *Acta Neuropathol* 2016; 131: 803-20.

Ma D, Gulani V, Seiberlich N, *et al*. Magnetic resonance fingerprinting. *Nature* 2013; 495: 187-92.

Marsan E, Baulac S. Review: Mechanistic target of rapamycin (mTOR) pathway, focal cortical dysplasia and epilepsy. *Neuropathol Appl Neurobiol* 2018; 44: 6-17.

McKenna A, Hanna M, Banks E, *et al*. The Genome Analysis Toolkit: a MapReduce framework for analyzing next-generation DNA sequencing data. *Genome Res* 2010; 20: 1297-303.

Mellerio C, Labeyrie MA, Chassoux F, *et al*. 3T MRI improves the detection of transmantle sign in type 2 focal cortical dysplasia. *Epilepsia* 2014; 55: 117-22.

Mirzaa GM, Campbell CD, Solovieff N, *et al*. Association of MTOR mutations with developmental brain disorders, including megalencephaly, focal cortical dysplasia, and pigmentary mosaicism. *JAMA Neurol* 2016; 73: 836-45.

Moller RS, Weckhuysen S, Chipaux M, *et al*. Germline and somatic mutations in the MTOR gene in focal cortical dysplasia and epilepsy. *Neurol Genet* 2016; 2: e118.

Najm IM, Sarnat HB, Blümcke I. Review: the international consensus classification of focal cortical dysplasia - a critical update 2018. *Neuropathol Appl Neurobiol* 2018; 44: 18-31.

Ribierre T, Deleuze C, Bacq A, *et al*. Second-hit mosaic mutation in mTORC1 repressor DEPDC5 causes focal cortical dysplasia-associated epilepsy. *J Clin Invest* 2018; 128: 2452-8.

Richards S, Aziz N, Bale S, *et al*. Standards and guidelines for the interpretation of sequence variants: a joint consensus recommendation of the American College of Medical Genetics and Genomics and the Association for Molecular Pathology. *Genet Med* 2015; 17: 405-24.

Rimmer A, Phan H, Mathieson I, *et al*. Integrating mapping-, assembly- and haplotype-based approaches for calling variants in clinical sequencing applications. *Nat Genet* 2014; 46: 912-8.

Robinson JT, Thorvaldsdottir H, Winckler W, *et al*. Integrative genomics viewer. *Nature Biotech* 2011; 29: 24-6.

Scheffer IE, Heron SE, Regan BM, *et al*. Mutations in mammalian target of rapamycin regulator DEPDC5 cause focal epilepsy with brain malformations. *Ann Neurol* 2014; 75: 782-7.

Urbach H, Scheffler B, Heinrichsmeier T, *et al*. Focal cortical dysplasia of Taylor's balloon cell type: a clinicopathological entity with characteristic neuroimaging and histopathological features, and favorable postsurgical outcome. *Epilepsia* 2002; 43: 33-40.

Vogelstein B, Papadopoulos N, Velculescu VE, Zhou S, Diaz Jr. LA, Kinzler KW. Cancer genome landscapes. *Science* 2013; 339: 1546-58.

Wagner J, Weber B, Urbach H, Elger CE, Huppertz HJ. Morphometric MRI analysis improves detection of focal cortical dysplasia type II. *Brain* 2011; 134: 2844-54.

Wang ZI, Alexopoulos AV, Jones SE, *et al*. Linking MRI postprocessing with magnetic source imaging in MRI-negative epilepsy. *Ann Neurol* 2014; 75: 759-70.

Wang ZI, Jones SE, Jaisani Z, *et al*. Voxel-based morphometric magnetic resonance imaging (MRI) postprocessing in MRI-negative epilepsies. *Ann Neurol* 2015; 77: 1060-75.